pH-Dependent Distribution of Chlorin e6 Derivatives across Phospholipid Bilayers Probed by NMR Spectroscopy

ARTICLE *in* LANGMUIR · JULY 2010

Impact Factor: 4.46 · DOI: 10.1021/la100679y · Source: PubMed

4 AUTHORS, INCLUDING:

Martina Vermathen
Universität Bern
22 PUBLICATIONS **515** CITATIONS
SEE PROFILE

Peter Vermathen
Inselspital, Universitätsspital Bern
99 PUBLICATIONS **1,859** CITATIONS
SEE PROFILE

Peter Bigler
Universität Bern
65 PUBLICATIONS **890** CITATIONS
SEE PROFILE

Langmuir
Article
pubs.acs.org/Langmuir

pH-Dependent Distribution of Chlorin e6 Derivatives across Phospholipid Bilayers Probed by NMR Spectroscopy

Martina Vermathen,*,† Mattia Marzorati,† Peter Vermathen,‡ and Peter Bigler†

†Department of Chemistry and Biochemistry, University of Bern, Freiestrasse 3, CH-3012 Bern, Switzerland, and ‡Department of Clinical Research (AMSM), MR-Center 1, University and Inselspital, CH-3010 Bern, Switzerland

Received February 15, 2010. Revised Manuscript Received April 7, 2010

The pH-dependent membrane adsorption and distribution of three chlorin derivatives, chlorin e6 (CE), rhodin G7 (RG), and monoaspartyl-chlorin e6 (MACE), in the physiological pH range (pH 6−8) were probed by NMR spectroscopy. Unilamellar vesicles consisting of dioleoyl-phosphatidyl-choline (DOPC) were used as membrane models. The chlorin derivatives were characterized with respect to their aggregation behavior, the pK_a values of individual carboxylate groups, the extent of membrane adsorption, and their flip-flop rates across the bilayer membrane for pH 6−8. External membrane adsorption was found to be lower for RG than for CE and MACE. Both electrostatic interactions and the extent of aggregation seemed to be the main determinants of membrane adsorption. Rate constants for chlorin transfer across the membrane were found to correlate strongly with the pH of the surrounding medium, in particular, for CE and RG. In acidic solution, CE and RG transfer across the membrane was strongly accelerated, and in basic solution, all compounds were retained, mostly in the outer monolayer. In contrast, MACE flip-flop across the membrane remained very low even at pH 6. The protonation of ionizable groups is suggested to be a major determinant of chlorin transfer rates across the bilayer. pK_a values of CE and RG were found to be between 6 and 8, and two of the carboxylate groups in MACE had pK_a values below 6. For CE and RG, the kinetic profiles at acidic pH indicated that the initial fast membrane distribution was followed by secondary steps that are discussed in this article.

Introduction

Photodynamic therapy (PDT) has become a widely accepted method for the treatment of cancer and several other nonmalignant diseases and is currently applied in various medical fields such as oncology, dermatology, and cosmetic surgery.[1] One of the major advantages of PDT is its site-specific selectivity achieved by the simultaneous combination of three components: the photosensitizer, light, and oxygen.[2,3] Porphyrinic photosensitizers are known to accumulate in diseased tissue with cellular membranes of various origins, such as the mitochondria or lysosomes, belonging to their main targets. Upon light irradiation of the sensitizer, the formation of cytotoxic species, mainly singlet oxygen but also other reactive oxygen species (ROS), is provoked, leading to cell damage.[4] Because of the short lifetime and high reactivity of singlet oxygen and ROS, the phototoxic reaction takes place at the location of their immediate formation (i.e., where the photosensitizer is located). With a diffusion coefficient of 2−4.7 $cm^2\ s^{-1}$ [5,6] and an intramembrane lifetime of 13−35 μs,[5] singlet oxygen can travel 60−100 nm/μs and thus rapidly exit from the membrane into the aqueous surroundings where its lifetime is even about 10-fold shorter. Therefore, the penetration of the photosensitizer into the membrane and its distribution within the membrane are crucial factors for PDT efficiency.[7] Accordingly, both cellular uptake and the subcellular localization of photosensitizers are reported to determine the PDT efficiency as well as the pathway of cell damage (e.g., necrosis or apoptosis).[8,9] More recently, intramembrane localization of porphyrinic photosensitizers has also become an important issue in a novel drug-delivery technology called photochemical internalization (PCI). PCI has evolved from PDT and is based on the same principles as PDT: the photosensitizer has to be located in the vesicular membrane to ensure the release of an entrapped drug by photochemical breakdown of the vesicle membrane after light irradiation.[10,11]

There is a common consensus with respect to which structural and physicochemical properties of a photosensitizer are favorable in PDT. Thus, light absorption maxima of photosensitizers are preferably shifted into the long-wavelength region to enable better tissue penetration of light,[12,13] a criterion that is met by chlorins because of their partially saturated ring systems.[14] In addition, amphiphilicity and a certain degree of hydrophobicity are

*Corresponding author. Tel: +41 031 631 4384. Fax: +41 031 631 3424. E-mail: martina.vermathen@ioc.unibe.ch.

(1) Hamblin, M. R.; Mroz, P. *Adv. Photodyn. Ther.: Basic, Translational, Clinical* **2008**, 1–12.
(2) MacDonald, I. J.; Dougherty, T. J. *J. Porphyrins Phthalocyanines* **2001**, *5*, 105–129.
(3) O'Connor, A. E.; Gallagher, W. M.; Byrne, A. T. *Photochem. Photobiol.* **2009**, *85*, 1053–1074.
(4) Castano, A. P.; Demidova, T. N.; Hamblin, M. R. *Photodiagnosis Photodyn. Ther.* **2004**, *1*, 279–293.
(5) Lavi, A.; Weitman, H.; Holmes, R. T.; Smith, K. M.; Ehrenberg, B. *Biophys. J.* **2002**, *82*, 2101–2110.
(6) Skovsen, E.; Snyder, J. W.; Lambert, J. D. C.; Ogilby, P. R. *J. Phys. Chem. B* **2005**, *109*, 8570–8573.
(7) Jimenez-Banzo, A.; Sagrista, M. L.; Mora, M.; Nonell, S. *Free Radical Biol. Med.* **2008**, *44*, 1926–1934.
(8) Kessel, D. *J. Porphyrins Phthalocyanines* **2004**, *8*, 1009–1014.
(9) Robertson, C. A.; Evans, D. H.; Abraharnse, H. *J. Photochem. Photobiol., B* **2009**, *96*, 1–8.
(10) Norum, O. J.; Selbo, P. K.; Weyergang, A.; Giercksky, K. E.; Berg, K. *J. Photochem. Photobiol., B* **2009**, *96*, 83–92.
(11) Berg, K.; Folini, M.; Prasmickaite, L.; Selbo, P. K.; Bonsted, A.; Engesaeter, B. O.; Zaffaroni, N.; Weyergang, A.; Dietze, A.; Maelandsmo, G. M.; Wagner, E.; Norum, O. J.; Hogset, A. *Curr. Pharm. Biotechnol.* **2007**, *8*, 362–372.
(12) Nyman, E. S.; Hynninen, P. H. *J. Photochem. Photobiol., B* **2004**, *73*, 1–28.
(13) Lang, K.; Mosinger, J.; Wagnerova, D. M. *Coord. Chem. Rev.* **2004**, *248*, 321–350.
(14) Juzeniene, A. *Photodiagnosis Photodyn. Ther.* **2009**, *6*, 94–96.

important for membrane penetration.[15,16] However, within this range of predefined properties, factors such as the exact membrane distribution, pathways of cellular uptake, and porphyrin self-association can turn out to be quite different in response to minor structural modifications or changes in pH and are still hard to predict for a given porphyrinic structure.

In particular, the pH value plays an important role in PDT, especially with porphyrinic photosensitizers bearing side chains that are ionizable in the physiological range. First, selective photosensitizer uptake by tumor tissue can be pH-driven because the interstitial fluid of tumor tissue often exhibits reduced pH as compared to normal tissue.[17,18] Second, the physicochemical properties of photosensitizers with carboxylic side chains can be different depending on their corresponding pK_a values and the pH of the surrounding medium. Lipophilicity and aggregate formation can both be strongly modified by the pH and represent factors that in turn determine cellular uptake and localization.[19] Therefore, there is currently great ongoing interest in understanding the factors modulating the interactions between photosensitizers and membranes, and several studies in this field have been carried out, mainly involving fluorescence spectroscopy.[20−25]

We previously demonstrated that NMR spectroscopy can also be efficiently used to understand the distribution process of different porphyrinic compounds within model membranes. The advantage of the NMR approach relies on the possibility not only to distinguish between the inner and outer layer of the phospholipid membrane but also to resolve various regions of the phospholipid components on a submolecular level within the membrane. Thus, changes undergone by these individual membrane regions can be directly monitored and resolved in a timely manner.[26]

The goal of the present study is to apply NMR spectroscopy to the investigation of pH effects in the physiological pH range on model membrane adsorption and the time-dependent distribution of three amphiphilic porphyrinic compounds with carboxylic side chains (Figure 1), namely, chlorin e6 (CE), rhodin G7 (RG), and monoaspartyl-chlorin e6 (MACE). In addition, factors such as chlorin aggregation and individual pK_a values of single carboxylate groups were probed for their influence on membrane interactions. The NMR spectroscopic data presented in this article enabled us to evaluate and understand the interplay and impact of mutually dependent factors such as chlorin structural modifications, pH effects, and aggregation on membrane incorporation and distribution.

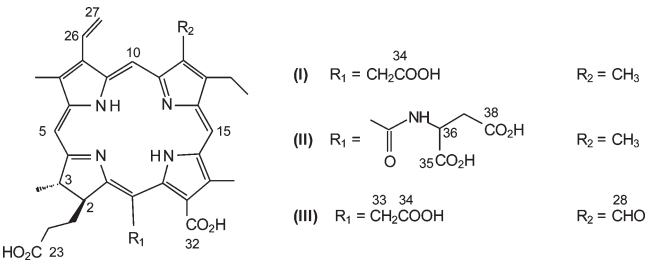

Figure 1. Structures of (I) chlorin e6 (CE), (II) monoaspartyl-chlorin e6 (MACE), and (III) rhodin G7 (RG).

Experimental Section

Materials. 18:1 PC (cis) 1,2-dioleoyl-*sn*-glycero-3-phosphocholine (DOPC) was purchased from Avanti Polar Lipids Inc. Chlorin e6 (CE), mono-L-aspartyl-chlorin e6 tetrasodium salt (MACE, Npe6), and rhodin G7 sodium salt (RG) were purchased from Frontier Scientific. The structures of CE, MACE, and RG are shown in Figure 1, and the structure of DOPC is shown in Figure 5. Deuterated solvents D_2O (D 99.9%), NaOD (40% in D_2O, D 99.5%), and DCl (20% in D_2O, D 99.5%) were obtained from Cambridge Isotopes Laboratories, Inc. Trimethyl-silyl-3-propionic acid sodium salt D4 (d_4-TMSP, D 98%), obtained from Euriso-Top, was used as an internal ^{1}H NMR reference, and 1,4-dioxane-d_8 (CU Chemie Uetikon AG) was used as an internal ^{13}C NMR reference. All chemicals and solvents were used without further purification. CE, MACE, and RG stock solutions were freshly prepared in D_2O at a concentration of 15 mM. Whereas MACE and RG existing as sodium salts could be directly dissolved in D_2O, chlorin e6 was first transferred into its sodium salt by adding NaOD solution. Phosphate-buffered saline (PBS) solutions with pH values between 6 and 8 were prepared by mixing different aliquots of 10 mM solutions of KH_2PO_4 and Na_2HPO_4 (both Sigma-Aldrich) in D_2O containing 0.9% NaCl.

Vesicle Preparation. Unilamellar DOPC vesicle (50−60 nm in diameter) solutions (10 mM DOPC) in PBS at different pH values between pH 6 and 8 were prepared by the extrusion method as previously described.[26]

Vesicle Loading with CE, MACE, and RG. A DOPC solution in PBS (500−600 μL, 10 mM) was transferred into 5 mm NMR tubes (Wilmad), and aliquots of CE, MACE, or RG stock solutions were added and mixed in the NMR tube to yield the desired molar ratio of chlorin/DOPC. Prior to each series of NMR measurements, the pH of each sample was measured directly in the NMR tube using a pH-electrode designed for NMR tubes (Spintrode 180 × 3 mm, Hamilton). The time between mixing of the chlorin stock solution with DOPC vesicles and the first NMR acquisition ("dead time") was about 10 min due to several preparation steps (e.g., pH measurement, matching and tuning of the NMR probe, locking-, and shimming procedure).

Nuclear Magnetic Resonance (NMR) Spectroscopy. The NMR experiments were performed on a Bruker Avance II spectrometer operating at a resonance frequency of 500.13 MHz for ^{1}H nuclei and 125.77 MHz for ^{13}C nuclei. The instrument is equipped with a 5 mm dual probe (BBI) for inverse detection with a *z*-gradient coil. All experiments were carried out at room temperature (298 K).

^{1}H NMR Spectroscopy. For time-dependent ^{1}H NMR measurements, a coaxial inner tube (WGS-5BL Wildmad) containing 60 μL of 1 mM TMSP in D_2O was inserted into each NMR sample tube as an internal reference. The ^{1}H NMR spectra were recorded using a 1D NOESY presaturation sequence with spoil gradients for residual water suppression ("noesygppr1d" from the Bruker pulse-program library). Typically 16 transients, a spectral width of 7352.9 Hz, 64 K data points, an acquisition time of 4.46 s, and a relaxation delay of 6 s were used to acquire the ^{1}H NMR

(15) Wiehe, A.; Shaker, Y. M.; Brandt, J. C.; Mebs, S.; Senge, M. O. *Tetrahedron* **2005**, *61*, 5535–5564.
(16) Rancan, F.; Wiehe, A.; Nobel, M.; Senge, M. O.; Al Omari, S.; Bohm, F.; John, M.; Röder, B. *J. Photochem. Photobiol., B* **2005**, *78*, 17–28.
(17) Pottier, R.; Kennedy, J. C. *J. Photochem. Photobiol., B* **1990**, *8*, 1–16.
(18) Gerweck, L. E.; Vijayappa, S.; Kozin, S. *Mol. Cancer Ther*. **2006**, *5*, 1275–1279.
(19) Cunderlikova, B.; Kaalhus, O.; Cunderlik, R.; Mateasik, A.; Moan, J.; Kongshaug, M. *Photochem. Photobiol*. **2004**, *80*, 373.
(20) Bronshtein, I.; Smith, K. M.; Ehrenberg, B. *Photochem. Photobiol*. **2005**, *81*, 446–451.
(21) Maman, N.; Brault, D. *Biochim. Biophys. Acta: Biomembranes* **1998**, *1414*, 31–42.
(22) Bonneau, S.; Maman, N.; Brault, D. *Biochim. Biophys. Acta, Biomembr*. **2004**, *1661*, 87–96.
(23) Mojzisova, H.; Bonneau, S.; Vever-Bizet, C.; Brault, D. *Biochim. Biophys. Acta, Biomembr*. **2007**, *1768*, 2748–2756.
(24) Mojzisova, H.; Bonneau, S.; Vever-Bizet, C.; Brault, D. *Biochim. Biophys. Acta, Biomembr*. **2007**, *1768*, 366–374.
(25) Lassalle, H. P.; Wagner, M.; Bezdetnaya, L.; Guillemin, F.; Schneckenburger, H. *J. Photochem. Photobiol., B* **2008**, *92*, 47–53.
(26) Vermathen, M.; Vermathen, P.; Simonis, U.; Bigler, P. *Langmuir* **2008**, *24*, 12521–12533.

spectra. The coadded free induction decays (FIDs) were exponentially weighted with a line-broadening factor of 1.0 Hz, Fourier transformed and phase corrected to obtain the ^{1}H NMR spectra.

^{13}C NMR Spectroscopy. For ^{13}C NMR chemical shift titration measurements, 1,4-dioxane was used as internal, pH-independent reference (δ_C = 67.6 ppm). The ^{13}C NMR spectra were recorded using a 1D sequence with power-gated ^{1}H decoupling ("zgpg" from the Bruker pulse-program library). Typically 1024 transients, a spectral width of 34 090.91 Hz, 64 K data points, an acquisition time of 0.96 s, and a relaxation delay of 4 s were used to acquire the ^{13}C NMR spectra. The free induction decays (FIDs) were exponentially weighted with a line-broadening factor of 5.0 Hz, Fourier transformed and phase corrected to obtain the ^{13}C NMR spectra. The chlorin carboxylate ^{13}C chemical shifts were assigned according to ^{1}H−^{13}C HMBC (heteronuclear multiple-bond connectivity) experiments.

Analysis of Time-Dependent Chlorin Distribution across the Bilayer. Time-dependent ^{1}H NMR spectra of DOPC−vesicle solutions were recorded after the addition of CE, MACE, or RG in molar ratios of 0.025 and 0.3 (chlorin/DOPC) at different pH values. The ^{1}H chemical shifts $\delta(t)$ of the DOPC inner $-N^+(CH_3)_3$, $(CH_2)_n$, and ω-CH_3 signals at time t after mixing were normalized to their initial values of $\delta_0(t = 0)$ (i.e., the chemical shift measured directly after mixing):

$$\delta_n(t) = \delta(t)/\delta_0(t = 0) \quad (1)$$

These $\delta_n(t)$ values were plotted as a function of time for each pH value and each compound. The distribution across the membrane may consist of more than a single step. To derive the rate constants for chlorin distribution across the membrane, a model was chosen for data fitting comprising three components: two exponentials and one sigmoidal component. The components were included in the fitting function used to calculate the normalized chemical shift $\delta_n(t)$:

$$\delta_n(t) = A(e^{(-t/t_1)} + We^{(-t/t_2)}) + \frac{S_1 - S_2}{1 + e^{(t-t_s)/t_3}} + S_2 \quad (2)$$

The fitting was applied simultaneously to all three DOPC resonances at a given pH with shared parameters for the time constants (t_1, t_2, t_3, and t_s) and the weighting factor W. These common parameters correspond to a model, assuming that the temporal chemical shift evolutions for the inner $-N^+(CH_3)_3$ and the inner acyl chain signals $(CH_2)_n$ and ω-CH_3 coherently proceed with the same rate constants and the same ratio of individual components. The independent parameters (A, S_1, and S_2) account for differences in the magnitude of temporal chemical shift changes for all three resonances. As opposed to an individual analysis for each DOPC resonance, the approach of dependent fitting is more powerful because it makes use of 3 times as many experimental data points. For some parameters, constraints were imposed: t_1, t_2, and t_3 were all enforced to be greater than zero. The sigmoidal part was constrained to suppress its impact on the initial signal evolution in order not to overlap strongly with the two exponential decays. This was done by enforcing t_s (i.e., the time offset of the sigmoidal function) to be greater than 80 h. Although the use of such constraints and fitting restricted to three components evolving in time reduces the possibility of obtaining spurious results, the model and results remain somewhat speculative. The kinetic steps to which the above model was applied are depicted in Figure 2 (steps 3 and 4). The plots in Figure 5 and 6 demonstrate that the calculated fitting curves yielded an overall suitable match to the measured data. For MACE at pH 6.25 (Figure 5, bottom left), only small shift changes were observed per time interval, leading to a larger variation of data points especially for the inherently broader lipid chain signals. The rate constants for the initial fast exponential decay of the normalized chemical shift were calculated from the fit results.

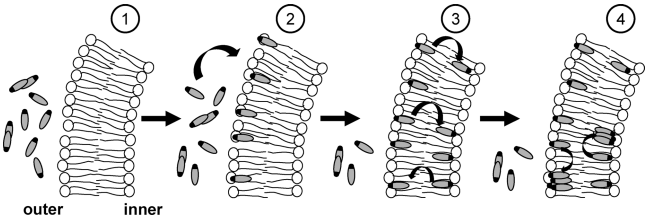

Figure 2. Steps of chlorin interaction with the phospholipid (PL) bilayer. (1) External addition of chlorin (at least partially aggregated) to chlorin-free vesicles. (2) Adsorption of chlorin molecules to the outer PL monolayer (t = 0, starting point of kinetic distribution studies). (3) Distribution of chlorin across the bilayer by flip-flop processes (kinetic process modeled by an exponential function). (4) Proposed secondary kinetic steps (modeled by a sigmoidal function) that may comprise intramembrane clustering of chlorin molecules.

pK_a Determination by ^{13}C NMR Spectroscopy.[27] Stock solutions (40 mM) of CE, MACE, and RG were prepared in saline (D_2O) and were adjusted to basic pH by adding a diluted NaOD/D_2O solution. The pH was then decreased stepwise by adding diluted 20% DCl/D_2O (1/50). After each titration step, the pH value was measured in an NMR tube and a ^{13}C NMR spectrum was acquired. The titration was stopped when the chlorin compound precipitated as indicated by a significant decrease in the ^{1}H NMR signal intensity. The observed ^{13}C chemical shifts of each carboxylate group were plotted as a function of pH. The data points were fitted according to the Henderson−Hasselbalch equation

$$\delta_{obs} = \frac{\delta_p + \delta_d 10^{(pH - pK_a)}}{1 + 10^{(pH - pK_a)}} \quad (3)$$

with δ_{obs}, δ_p, and δ_d being the ^{13}C chemical shifts of the observed, the protonated, and the deprotonated species of the corresponding chlorin compound, respectively. Even though the complete titration curves could not be obtained because of aggregation in acidic solution, sufficient data points could be acquired to obtain good fitting results. The pK_a values were derived from eq 3. pD/pH corrections were not performed but have to be taken into account when comparing with literature values reported for H_2O solutions.[27]

Postprocessing of the NMR spectra was performed using Bruker software Topspin 2.1. Fitting procedures were carried out using Origin, version 5.0 (Microcal Software, Inc.). The Levenberg−Marquardt algorithm was applied to minimize the sum of the squares.

Results

The different steps involved in chlorin membrane interaction presented in this paper are summarized and delineated in Figure 2. The proposed single processes as concluded from our data will be outlined in the following.

^{1}H NMR Spectra of DOPC Vesicles after Chlorin Addition and of Pure Chlorins in PBS. The external addition of porphyrinic compounds to DOPC vesicles can induce characteristic perturbations to the ^{1}H NMR spectrum of the phospholipids assembled in a bilayer. These perturbations are assumed to be mainly due to the strong porphyrin ring current effects on the DOPC protons in close proximity. Therefore, DOPC protons located either above or below the porphyrin macrocycle plane experience upfield shifts of their corresponding ^{1}H NMR signals, as has been previously shown for CE and MACE.[26] The most

(27) Popov, K.; Ronkkomaki, H.; Lajunen, L. H. J. *Pure Appl. Chem.* **2006**, *78*, 663–675.

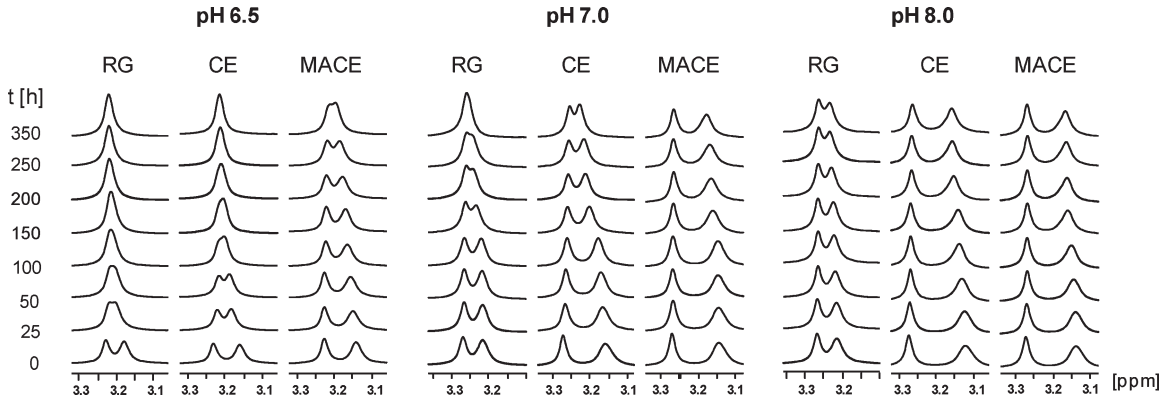

Figure 3. ^{1}H NMR spectra of DOPC $-N^+(CH_3)_3$ signals at various time points after the addition of RG, CE, and MACE to DOPC vesicles (molar ratio of chlorin/DOPC = 0.025) at pH 6.5, 7, and 8.

Table 1. Chemical Shift Difference $\Delta\delta$ of DOPC Inner and Outer $N^+(CH_3)_3$ Signals after the Addition of RG, CE, or MACE[a]

	$\Delta\delta$ (ppm)		
pH	RG	CE	MACE
6.5	0.0491	0.0698	0.0844
7.0	0.0524	0.1135	0.1247
8.0	0.0528	0.1502	0.1333

[a] Mole ratio of chlorin/DOPC = 0.025.

pronounced change, observed in this study immediately after the addition of either RG, CE, or MACE to DOPC vesicles, was a split of the DOPC $-N^+(CH_3)_3$ signal indicating fast adsorption of the porphyrin to the bilayer surface (Figure 2, step 2). Figure 3 shows the split choline signals in the corresponding DOPC vesicle ^{1}H NMR spectra. The signal at higher field (smaller ppm value) corresponds to DOPC choline protons located in the outer membrane layer (i.e., in proximity to the porphyrin), and the signal at lower field corresponds to the initially unperturbed DOPC choline protons from the inner membrane layer. We have previously shown that the chemical shift difference of the two DOPC inner and outer $-N^+(CH_3)_3$ signals correlates with the amount of porphyrin bound to the vesicles. The initial shift differences $\Delta\delta$ observed right after mixing the same amounts of each of the three chlorin compounds (0.25 mM) with DOPC vesicles (10 mM) are listed in Table 1. RG induces the smallest split rather independently of pH within the range of interest (average $\Delta\delta = 0.0514 \pm 0.0015$ ppm), indicating at first glance a lower affinity for the vesicles as compared to the vesicle affinity exhibited by CE and MACE. Both CE and MACE induce larger shift differences of the split choline signal with increasing pH, indicating increasing membrane adsorption at the vesicle surface.

Differences in the aggregation behavior seem to be the main contributor to the different membrane affinities besides the variations in structure and ionic state. The ^{1}H NMR spectra of the pure chlorins in PBS (Figure 4) provide information on the approximate extent of aggregate formation. In Figure 4, the aromatic regions of the ^{1}H NMR spectra of RG, CE, and MACE are shown at different pH values. As compared to CE and MACE, the ^{1}H signals of RG in part exhibit stronger line broadening (e.g., H-5 and H-26), suggesting the existence of larger self-associates. Moreover and in contrast to CE and MACE, the spectra for RG are very similar at pH 6.5, 7, and 8 with respect to peak positions whereas peak integrals (determined between 8 and 10 ppm) drop from 100% at pH 8 to 64% at pH 6.5. This signal loss is most likely due to the formation of very

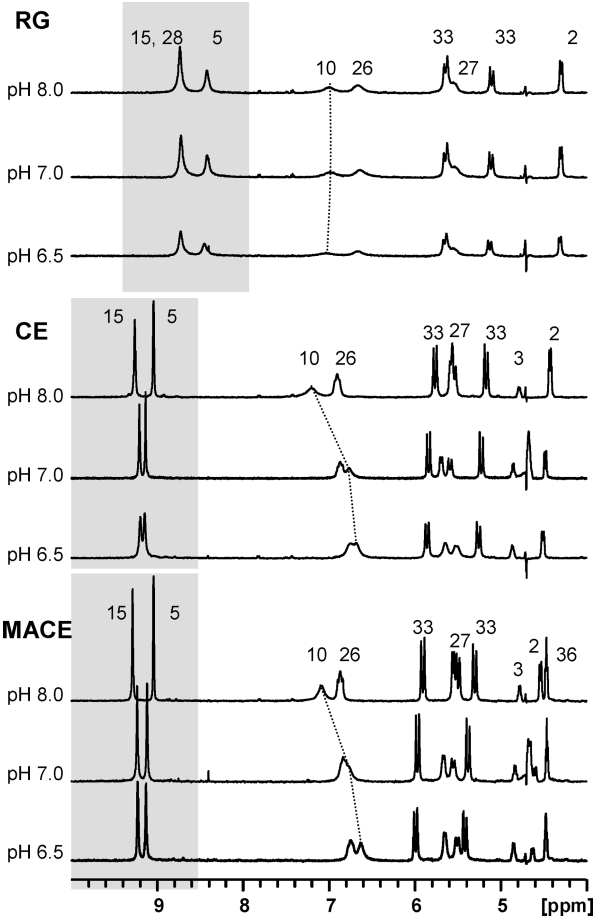

Figure 4. Aromatic region of the ^{1}H NMR spectra of 2.5 mM RG, CE, and MACE in PBS at pH 6.5, 7, and 8. Regions for integration are highlighted.

large aggregates that do not give rise to NMR signals.[28,29] For CE and MACE, the corresponding integrals drop only to 88 and 94%, respectively, at pH 6.5. The majority of peaks in the CE and MACE spectra are narrow and well-resolved. However, the existence of, most likely, oligomers is indicated by

(28) Rubires, R.; Crusats, J.; El Hachemi, Z.; Jaramillo, T.; Lopez, M.; Valls, E.; Farrera, J. A.; Ribo, J. M. *New J. Chem.* **1999**, *23*, 189–198.
(29) Hosomizu, K.; Oodoi, M.; Umeyama, T.; Matano, Y.; Yoshida, K.; Isoda, S.; Isosomppi, M.; Tkachenko, N. V.; Lemmetyinen, H.; Imahori, H. *J. Phys. Chem. B* **2008**, *112*, 16517–16524.

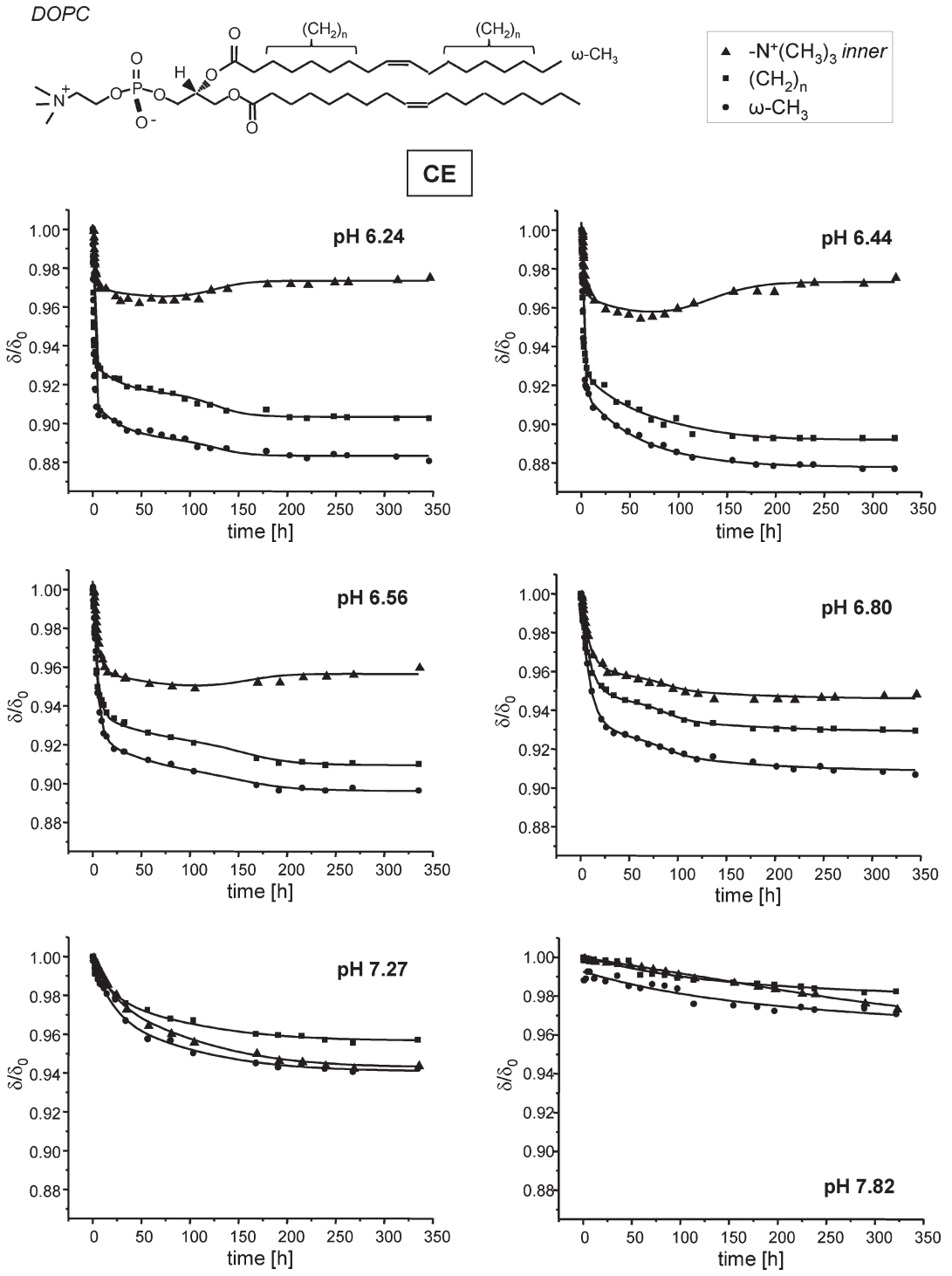

Figure 5. Normalized chemical shift δ/δ_0 of DOPC inner choline $-N^+(CH_3)_3$ (▲), $-(CH_2)_n$ (■), and ω-CH_3 (●) resonances as a function of time after the addition of CE at various pH values. The molar ratio of CE/DOPC is 0.3. Solid lines correspond to fitting curves (fitting function: Experimental Section).

ring-current-induced signal broadening and shifts of certain protons (e.g., H-10).[30] As the pH is increased from 6.5 to 8, these signals experience characteristic downfield shifts toward their theoretical monomer position, indicating disaggregation.[31]

Time-Resolved ^{1}H NMR Spectra of DOPC Vesicles after Chlorin Addition at Various pH Values. Once attached to the membrane surface, the distribution of a porphyrinic compound across the bilayer can be monitored by temporal follow-up of the DOPC vesicle ^{1}H spectra. This distribution process is depicted in Figure 2, step 3. As an increasing number of chlorin molecules reaches the inner membrane layer, the initially unperturbed inner choline signal becomes upfield shifted while the outer signal simultaneously shifts downfield because of chlorin depletion in the outer membrane layer. Inner and outer choline signals finally merge when equilibrium is reached, whereas a remaining split probably indicates an asymmetric distribution. Time-resolved

(30) Abraham, R. J.; Smith, K. M. *J. Am. Chem. Soc.* **1983**, *105*, 5734–5741.
(31) Gomi, S.; Nishizuka, T.; Ushiroda, O.; Uchida, N.; Takahashi, H.; Sumi, S. *Heterocycles* **1998**, *48*, 2231–2243.

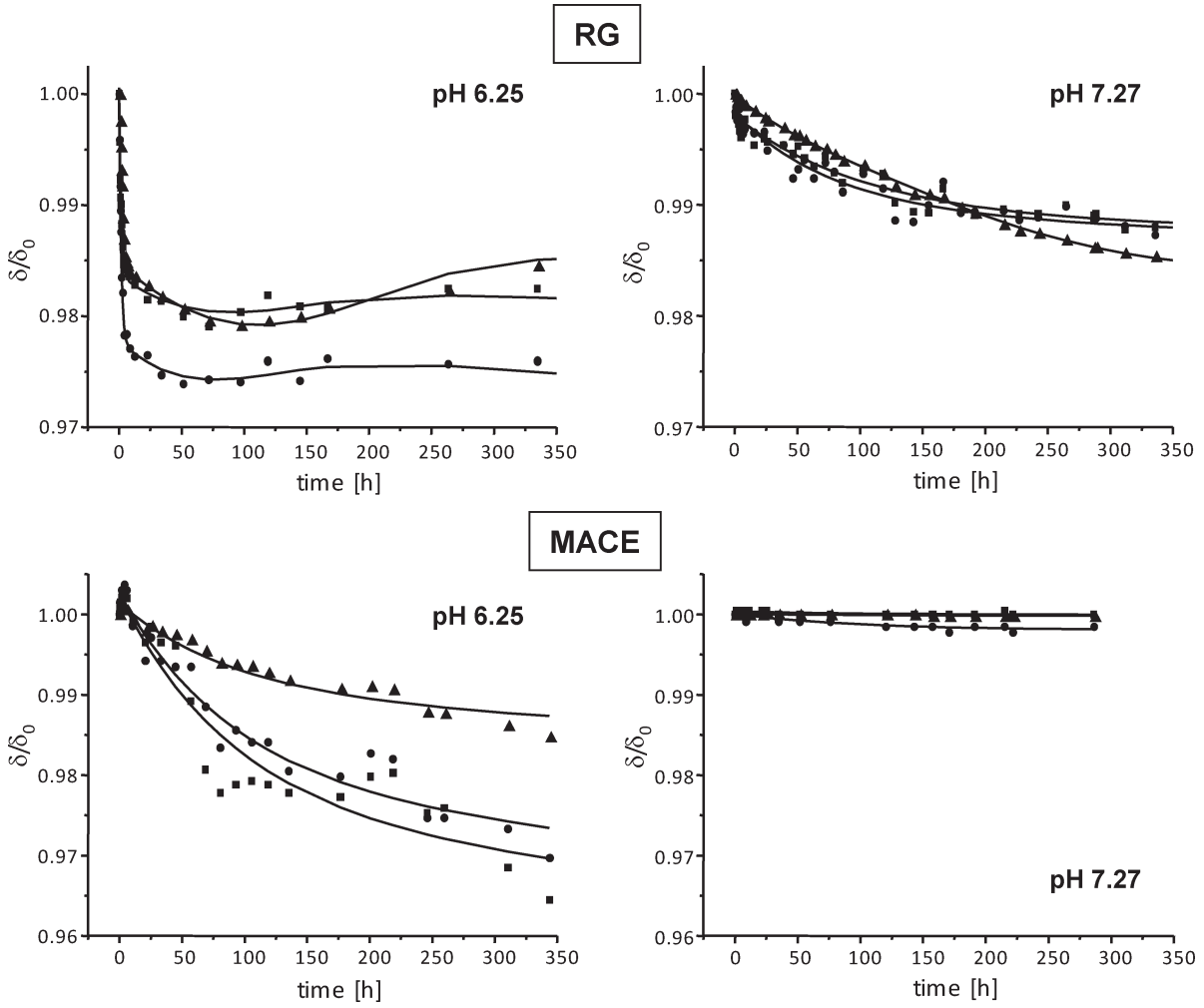

Figure 6. Normalized chemical shift δ/δ_0 of DOPC inner choline $-N^+(CH_3)_3$ (▲), $-(CH_2)_n$ (■), and ω-CH_3 (●) resonances as a function of time after the addition of RG and MACE at pH 6.25 and 7.27. The molar ratio of chlorin/DOPC is 0.3. Solid lines correspond to fitting curves (fitting function: Experimental Section).

^{1}H NMR spectra of DOPC vesicles after the addition of each of the chlorin compounds (RG, CE, and MACE) were acquired at pH 6.5, 7, and 8, covering the physiological pH range. The corresponding spectra (i.e., the region of the DOPC choline signals) are shown in Figure 3. Comparing the different pH values, at pH 6.5, the inner and outer choline peaks merge in the observed time frame in the presence of RG and CE and also nearly merge with MACE, indicating an approximately equal distribution of chlorins between the two monolayers. At pH 8, however, the split choline signals remain separated for all chlorin compounds, suggesting an asymmetric distribution between the two membrane layers. The chlorin molecules remain more or less attached to the outer membrane layer, and only a few are able to cross the bilayer. This is still the case for MACE at pH 7, whereas CE and RG slowly distribute across the bilayer. The residual shift difference observed for CE but not for RG at the end point of the time interval may be partially attributed to the different amounts of CE and RG initially adsorbed at the vesicle surface. The smaller amount of adsorbed RG, as concluded above from the initial $\Delta\delta$ value (Table 1), will be more quickly distributed across the bilayer.

Rate Constants for Membrane Distribution at Various pH Values. To derive rate constants for the pH-dependent membrane distribution kinetics, a time-dependent follow-up of the DOPC−vesicle ^{1}H NMR spectra was recorded after the addition of each of the chlorin compounds at increased chlorin concentrations (molar ratio of chlorin/DOPC = 0.3) at different pH values. At increased chlorin concentration, the induced shift changes observed for the DOPC signals are larger, thereby simplifying the kinetic analysis. At a molar ratio of 0.025 (chlorin/DOPC) chlorin transfer across the bilayer seems to follow first-order kinetics. This may also be assumed at a molar ratio of 0.3, at least for the first, most important step (i.e., chlorin uptake by the initially chlorin-free inner membrane layer from the chlorin pool bound to the outer layer). Three of the main signals in the DOPC ^{1}H NMR spectrum, as previously shown,[26] were evaluated: the inner $-N^+(CH_3)_3$, the acyl chain $-(CH_2)_n$, and the (inner, if applicable) ω-CH_3 resonances. In Figure 5, plots of normalized chemical shifts δ/δ_0 of the corresponding DOPC signals versus time are shown for selected pH values recorded after mixing DOPC vesicles with CE. In Figure 6, the corresponding data are shown for RG and MACE, each at acidic and neutral pH.

By comparing the different pH values, the following observations can be made for all three chlorin compounds: (i) The time-dependent changes are strongly pH-dependent in terms of magnitude, type, and rate. (ii) With increasing pH, the overall membrane distribution rate is slower. (iii) The overall magnitude of chemical shift changes (i.e., the maximum displacement $\Delta_{max}(\delta/\delta_0)$), especially for the lipid chain signals, decreases

with increasing pH. (iv) Apart from absolute values, the temporal progression for the three signals of interest run parallel for each pH value (i.e., relative changes for the inner $-N^+(CH_3)_3$ resonance and the $(CH_2)_n$ and ω-CH_3 acyl-chain signals occur simultaneously). At pH values below 7, the temporal progression of δ/δ_0 occurs to be clearly triphasic for CE and RG. The first stage is characterized by a steep decrease in δ/δ_0 values, which is slowed down in the second stage. The third segment appears at time values above ~100 h and is distinguished by an apparently sigmoidal progression of δ/δ_0 data points with opposite signs for the inner $-N^+(CH_3)_3$ resonance on one hand and the $(CH_2)_n$ and ω-CH_3 acyl-chain signals on the other hand. Whereas the chemical shift of the inner $-N^+(CH_3)_3$ signal first moves upfield and then slightly back downfield, the $(CH_2)_n$ and ω-CH_3 acyl-chain signals continuously move upfield.

To derive the rate constants, the data were fit by applying a three-component model (Experimental Section) to account for the subsequent steps observed. The calculated fitting curves, shown as solid lines in Figures 5 and 6, yielded a suitable match to the measured data.

Other than CE, δ/δ_0 values for RG changed much less. For MACE, δ/δ_0 values remained nearly unchanged at neutral pH and decayed only weakly at pH 6.25 (Figure 6).

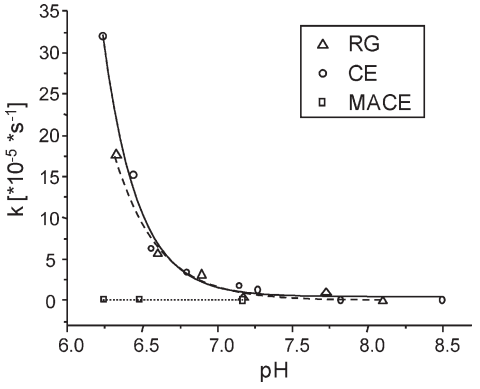

Figure 7. Rate constant k as a function of pH for RG (Δ), CE (○), and MACE (□) added to DOPC vesicles. The molar ratio of chlorin/DOPC is 0.3. Lines correspond to fitting of the data to an exponential decay function.

Because the major part of membrane-bound chlorin apparently partitions between the two monolayers during the first stage, the rate constants k for the initial fast exponential decay of the normalized chemical shift were calculated from the fit results and plotted as a function of pH (Figure 7). For CE and RG, k is similar and decreases exponentially with increasing pH for the investigated pH range. Between pH 6 and 7, the distribution process is slowed down by about an order of magnitude. In basic solution (pH around 8), almost no partitioning between the inner and outer monolayers takes place anymore. For MACE, the rate constant remains very low, even at pH around 6.

pK_a Determination by ^{13}C NMR Spectroscopy. To test whether different pK_a values account for the differences found for the pH dependence of membrane distribution kinetics, these values were determined for CE, RG, and MACE by ^{13}C NMR spectroscopy. ^{13}C chemical shift titration allows for the simultaneous pK_a determination of the individual carboxylate groups for each chlorin compound. This is exemplified for MACE in Figure 8. The region of the ^{13}C NMR spectrum of MACE in D_2O is shown where the ^{13}C signals of the carboxylate groups occur. Plots of the corresponding ^{13}C chemical shifts as a function of pH can be used to obtain the pK_a values from fitting the data points according to the Henderson−Hasselbalch equation (Experimental Section). The pK_a values obtained for the individual carboxylate groups of CE, RG, and MACE are listed in Table 2. The pK_a value of the COOH-35 group in MACE had to be estimated (~4), and also the other values are somewhat uncertain because of aggregation in the low-pH range. Nevertheless, it is obvious that the two additional carboxylate groups (COOH-35 and COOH-38) introduced with the aspartyl residue in MACE are clearly more acidic than the residual carboxylate groups (COOH-23 and COOH-32) and the carboxylate groups in CE and RG. Whereas for CE and RG the pK_a values fall into the pH range between 6.5 and 8.5, the two aspartyl carboxylate groups of MACE are still deprotonated in this range.

Table 2. pK_a Values of Chlorin Carboxylate Groups

	pK_a				
	COOH-23	COOH-32	COOH-34	COOH-35	COOH-38
RG	6.8 ± 0.4	7.3 ± 0.3	6.7 ± 0.1		
CE	7.9 ± 0.1	8.3 ± 0.1	7.9 ± 0.1		
MACE	6.2 ± 0.1	7.8 ± 0.1		~4	5.6 ± 0.1

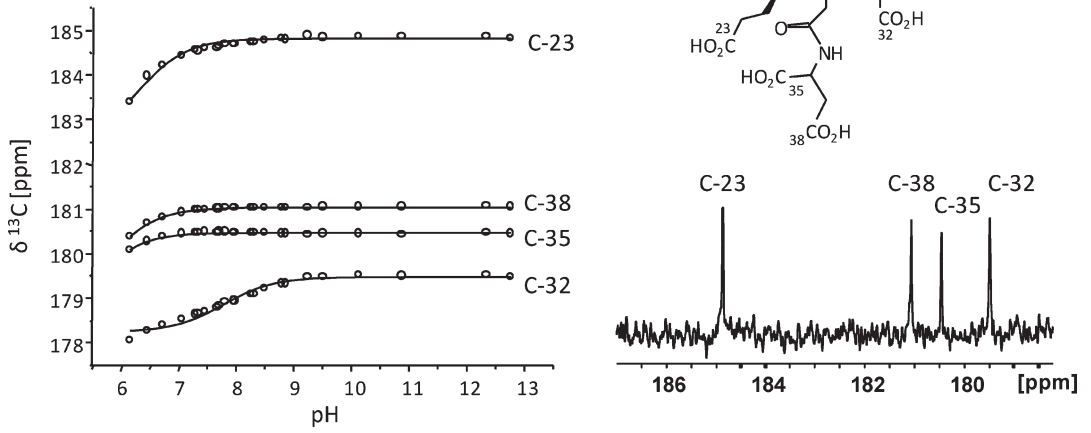

Figure 8. pK_a determination for MACE carboxylate groups by ^{13}C NMR chemical shift titration as a function of pH. Lines correspond to fitting of the data according to the Henderson−Hasselbalch equation (Experimental Section).

Discussion

The characterization of porphyrin interactions with phospholipid bilayers involves two main aspects: the affinity of porphyrin for the bilayer (Figure 2, steps 1 and 2) and the distribution of porphyrin within the bilayer (Figure 2, steps 3 and 4). The data presented in this article indicate that both processes seem to be strongly modified by the porphyrin structure, the pH value, and the aggregation behavior.

pH-Dependent Membrane Affinity and Aggregation. All three chlorin derivatives investigated in this study bear ionizable carboxylic side chains on one side of the porphyrin macrocycle whereas the opposite side is rather nonpolar. In general, this amphiphilicity favors both porphyrin self-association[32] and membrane association.[4,9,32] In this study, the affinity for membrane adsorption was found to be lower and rather pH-independent for RG, but it increased with pH for CE and MACE in the investigated range between pH 6 and 8. These observed differences between RG on one side and CE and MACE on the other seem to be governed mainly by differences in the aggregation behavior. Because CE and RG have similar pK_a values (Table 2), observed differences in aggregation must in turn be due to the structural difference (i.e., the introduction of an aldehyde group into the hydrophobic side in RG compared to CE). ^{1}H NMR spectra of porphyrins in water can provide semiquantitative information on the aggregate size as well as qualitative information on the aggregate structure. Thus, the larger the aggregates, the more signal broadening that occurs, whereas specific broadening of only certain signals and characteristic "unusual" shifts indicate overlapping sites (i.e., aggregate-forming sites).[31,33] The extent of aggregation was larger for RG than for CE and MACE (Figure.4). First, the ^{1}H signals of "NMR-visible" RG aggregates exhibited stronger signal broadening, and no changes with respect to the chemical shift and line width occur between pH 6 and 8 (Figure 4). Second, besides the existence of these smaller aggregates, significant aggregate growth at acidic pH is indicated by the overall signal loss at pH 6.5 (Figure 4). The lack of changes in RG adsorption to the membrane despite this aggregate growth suggests that the membrane affinity is mainly determined by the constant fraction of smaller aggregates or oligomers. The size and structure of these oligomers seem to remain unaffected within the investigated pH range and seem to be responsible for the correspondingly unchanged low membrane affinity of RG. On the contrary, CE and MACE exhibited increasing membrane adsorption with increasing pH from 6.5 to 8 (Table 1). Increasing deprotonation of the carboxylate groups may partially account for this finding. The importance of electrostatic interactions in porphyrin membrane adsorption has been previously proposed on the basis of micellar studies.[34,35] Likewise, electrostatic interactions have been reported to be responsible for anchoring amphiphilic porphyrins in the phospholipid membrane headgroup region with the hydrophobic moiety protruding into the nonpolar membrane interior.[20,32]

In addition to deprotonation, the pH increase seems to induce disaggregation for MACE and CE as indicated by the observed changes in the ^{1}H NMR spectra of CE and MACE in PBS (Figure 4). This decreased aggregation most likely enhances the membrane association ability at higher pH values whereas highly aggregated species that do not give rise to detectable NMR signals hardly attach to the membrane (supported by own unpublished results). In accordance with our data, it has been shown for azaphthalocyanines that strong aggregation forces may significantly reduce vesicle incorporation and that the stability of aggregates largely depends on the nature of the substituents.[36] Whereas even large aggregates can be internalized into cells by endocytosis, as has been shown for the methyl esters of pyropheophorbide-a and chlorin e6, their intracellular distribution was also found to depend on the degree of aggregation.[37] Thus, membrane adsorption between pH 6 and 8 seems to be governed by both the extent of deprotonation of the carboxylic side chains (i.e., electrostatic interactions) and the extent of aggregation that on one hand correlates with deprotonation but on the other hand also depends on the nature of nonionizable substituents.

pH Dependence of the Membrane Distribution Rate. The discussion so far concerned the obviously very fast adsorption of chlorin compounds on the membrane right after their addition to vesicles (Figure 2, steps 1 and 2) (i.e., without regarding subsequent steps). This is the starting point for studying the time-dependent membrane distribution (Figure 2, steps 3 and 4), which will be discussed in the following text.

Rate constants for CE and RG transfer across the membrane were found to decrease strongly with the increasing pH of the surrounding medium (Figure 7). However, for MACE, pH changes had only a small effect on membrane distribution occurring at a uniformly low rate within the examined range. In basic solution, all compounds were retained mostly in the outer monolayer.

Differences in the pK_a values determined for the three chlorin derivatives most likely account for the observed differences in the membrane distribution of CE and RG on one side and MACE on the other side. Whereas all three pK_a values of the carboxylate groups in CE and RG were found to be between pH 6.5 and 8.5 (Table 2), the additional aspartyl-carboxylate groups in MACE introduce a more acidic moiety with a pK_a value of around 4 or 5. According to these results, the protonation of CE and RG carboxylic side chains significantly facilitates the distribution between the inner and outer membrane hemisphere. In MACE, however, the two aspartyl-carboxylate groups are still mainly deprotonated at pH 6 and thus seem to be responsible for the strong binding of MACE to the phospholipid headgroups of the outer membrane layer by electrostatic interactions. These results constitute the most important finding of this study suggesting that the pH-controlled extent of protonation of ionizable groups generally has a major effect on flip-flop rate constants, making it easier for the corresponding molecule in its protonated form to pass the hydrophobic interior of the membrane. In agreement with this, the flip-flop rate of deuteroporphyrin (DP) has been reported to be increased by about 3 orders of magnitude when reducing the pH from 8.5 to 6.5.[21,38] Likewise, rate constants for flip-flop processes across model membranes of other compounds bearing acidic groups, such as bile acids[39] and fatty acids,[40] were found to depend similarly on pH. Comparable to MACE,

(32) Kepczynski, M.; Pandian, R. P.; Smith, K. M.; Ehrenberg, B. *Photochem. Photobiol.* **2002**, *76*, 127–134.
(33) Koehorst, R. B. M.; Hofstra, U.; Schaafsma, T. J. *Magn. Reson. Chem.* **1988**, *26*, 167–172.
(34) Vermathen, M.; Louie, E. A.; Chodosh, A. B.; Ried, S.; Simonis, U. *Langmuir* **2000**, *16*, 210–221.
(35) Santiago, P. S.; Neto, D. D.; Gandini, S. C. M.; Tabak, M. *Colloids Surf., B* **2008**, *65*, 247–256.
(36) Zimcik, P.; Miletin, M.; Kopecky, K.; Musil, Z.; Berka, P.; Horakova, V.; Kucerova, H.; Zbytovska, J.; Brault, D. *Photochem. Photobiol.* **2007**, *83*, 1497–1504.
(37) Kelbauskas, L.; Dietel, W. *Photochem. Photobiol.* **2002**, *76*, 686–694.
(38) Bonneau, S.; Vever-Bizet, C.; Mojzisova, H.; Brault, D. *Int. J. Pharm.* **2007**, *344*, 78–87.
(39) Cabral, D. J.; Small, D. M.; Lilly, H. S.; Hamilton, J. A. *Biochemistry* **1987**, *26*, 1801–1804.
(40) Kamp, F.; Hamilton, J. A. *Proc. Natl. Acad. Sci. U.S.A* **1992**, *89*, 11367–11370.

fluorescence studies on a disulfonated phthalocyanine ($AlPcS_2$) have shown that this compound did not permeate the membrane, which was attributed to the charged sulfonate groups.[38]

In contrast to our finding, carboxylic groups' pK_a values for CE have been predicted to be between 4.4 and 4.9,[32] although these values were not derived from experimental data. However, the concentration and aggregation state, both interdependent parameters, may cause different pK_a values, and often a wide variation in reported pK_a values is found in the literature for porphyrins.[17] It is therefore important to note that absolute pK_a values depend on the exact experimental conditions, although this does not affect the relative differences observed under the same conditions such as those between the three chlorin derivatives. Nevertheless, a number of different findings support our conclusion that between pH 6 and 8 major changes in lipophilicity take place for CE and RG as is reflected by their pK_a values, coinciding with large changes in membrane distribution rates and aggregation behavior within this range: Effective modifications of CE have been reported to occur in the physiological pH region of 6−8, as was derived from inflection points at around pH 6.5 from spectrophotometric and fluorimetric titration curves of CE in PBS[41] and at around pH 7.4 in the presence of human plasma.[42] Furthermore, log P (octanol−water partition coefficient) values for CE were found to increase with decreasing pH within the physiological pH range (6−8) from about 10 at pH 6.7 to about 3 at pH 7.6.[41] Likewise, for chlorin p6, significant changes have been reported to occur within the physiological pH range (i.e., increasing hydrophobicity and consequently increased aggregation with a slight pH decrease).[43] Accordingly, chlorin p6 was found to be photodynamically more effective in a hydrophobic environment despite enhanced aggregation at acidic pH (5 to 6).[44]

When comparing the three chlorin derivatives with respect to their membrane distribution rates, it has to be taken into account that according to their different pH-dependent membrane affinities different amounts of chlorin reside in the outer membrane layer at the starting point. In fact, we have previously shown that this distribution rate is slightly increased with increasing amount of porphyrin inside the membrane.[26] However, the observed pH-induced rate changes reported here are much larger (up to 2 orders of magnitude) so that they cannot simply be attributed to a concentration increase. Moreover, a comparison of the time evolutions at low (Figure 3) and high (Figure 5, 6) chlorin concentrations confirmed that similar correlations apply between the pH and membrane distribution rate, independently of the absolute amount of chlorin inside the membrane (results not shown in detail).

There are several reports proposing that, within certain limits, with increasing hydrophobicity or log P value of a porphyrin the membrane incorporation and cellular uptake are enhanced.[20,32,45] In contrast, a negative correlation between log P values (>8) of very hydrophobic porphyrins and passive diffusional liposome uptake has been reported.[46] Our data suggest that, amphiphilicity provided, an increase in negatively charged groups, namely, $-COO^-$, along with low aggregation rather promotes outer membrane association (i.e., the initial step). However, the kinetic data show that such charged species (e.g., MACE at pH 6−8 and CE and RG at pH 8) remain anchored in the outer membrane layer. Protonated chlorin species, however, move partially toward the inner layer to establish equilibrium. This in turn enables the outer layer to take up additional chlorin from the surrounding medium, thereby increasing the overall amount of porphyrin incorporated by the membrane. Our data demonstrate that it is important to probe membrane entry and membrane distribution separately because parameters such as the number of carboxylic groups at corresponding pK_a values seem to determine the corresponding degree differently.

Membrane Localization and Secondary Time-Evolution Steps. A detailed analysis of the time evolution including the behavior of $-N^+(CH_3)_3$, $-(CH_2)_n$, and ω-CH_3 proton signals at various pH values, as shown for CE in Figure 5, provides information not only on the phospholipid headgroup but also on the lipid chain regions. Furthermore, it suggests that secondary steps follow the initial fast distribution, especially at lower pH.

The overall magnitude of relative chemical shift changes (δ/δ_0 values) for the lipid chain signals ($-(CH_2)_n$ and ω-CH_3) clearly increased with decreasing pH (Figure 5). This suggests that a decrease in pH not only significantly accelerates CE flip-flop but also favors CE molecules residing deeper in the hydrophobic region of the membrane. As a result, more CE molecules are in closer proximity to the DOPC lipid chains at equilibrium, leading to larger changes in the corresponding NMR signals. In agreement with these results, such a pH-dependent vertical displacement within the membrane (i.e., a deeper penetration into the lipid region in an acidic medium) has also been proposed for chlorin[47] and for hematoporphyrin (HP) derivatives derived from fluorescence studies.[20]

Whereas at neutral or higher pH data points can be satisfactorily fitted by single exponentials, in acidic solution the temporal evolutions of data points exhibit a pronounced triphasic character implying specific secondary steps following the initial fast chlorin distribution (Figure 5 for CE at pH <6.8 and Figure 6 for RG at pH 6.25). Therefore, the applied fitting procedure was based on a corresponding kinetic model involving three temporal progression steps (Experimental Section). These three different kinetic steps could be described by the same time constants for all three DOPC resonances at a given pH value, supporting the assumption that the observed changes are correlated and take place simultaneously. Nevertheless, the model and the subsequent interpretation remain speculative.

Because low pH promotes the self-association of chlorin, this feature may significantly modulate membrane-transfer kinetics. Therefore, it can be assumed that at low pH self-association and membrane incorporation are competing processes. The rate constant k for the first phase may thus be attributed to the fast flip-flop of protonated and thus more hydrophobic CE monomers. This process is presumably slowed down by CE self-association leading to the second slower phase. Contributions to the second rate constant may originate from both aggregate growth in the aqueous bulk phase, slowing down the release of CE molecules for membrane incorporation, and the presence of dimers or oligomers within the membrane exhibiting decreased flip-flop rates. To date, it is still unclear whether porphyrins incorporate exclusively in their monomer state or whether they

(41) Cunderlikova, B.; Gangeskar, L.; Moan, J. *J. Photochem. Photobiol., B* **1999**, *53*, 81–90.
(42) Cunderlikova, B.; Kongshaug, M.; Gangeskar, L.; Moan, J. *Int. J. Biochem. Cell Biol.* **2000**, *32*, 759–768.
(43) Datta, A.; Dube, A.; Jain, B.; Tiwari, A.; Gupta, P. K. *Photochem. Photobiol.* **2002**, *75*, 488–494.
(44) Bose, B.; Dube, A. *J. Photochem. Photobiol., B* **2008**, *93*, 32–35.
(45) Henderson, B. W.; Bellnier, D. A.; Greco, W. R.; Sharma, A.; Pandey, R. K.; Vaughan, L. A.; Weishaupt, K. R.; Dougherty, T. J. *Cancer Res.* **1997**, *57*, 4000–4007.
(46) Ben Dror, S.; Bronshtein, I.; Wiehe, A.; Röder, B.; Senge, M. O.; Ehrenberg, B. *Photochem. Photobiol.* **2006**, *82*(3), 695–701.
(47) Zorin, V.; Michalovsky, I.; Zorina, T.; Khludeyev, I. *Proc. SPIE* **1996**, *2625*, 146–155.

also exist as oligomers inside membranes and if so, to what extent.[37]

Although still tentative, a process that may be considered to cause the third sigmoidal-type phase is the possibility of aggregate growth inside the bilayer phase as is depicted in Figure 2, step 4. Even though the surroundings of ordered phospholipid molecules allow only restricted motion, it may be possible that chlorin incorporated into the bilayer as a monomer may exhibit slow, restricted self-association in the membrane, resulting in chlorin-enriched domains. The possibility of porphyrin self-aggregate formation within membranes has been described by several authors.[48,49] Moreover, the kinetics of aggregate formation has in several cases been reported to follow a sigmoidal time evolution similar to that in our proposed model.[50,51] Nevertheless, it is presumed that, apart from aggregation, the integrity of the membrane-incorporated chlorin compounds is maintained throughout the experimental setup. This was supported by the stable green color observed for all chlorin-containing vesicle solutions, unchanged light absorption spectra, and no occurrence of any degradation products in the NMR spectra of these solutions.

Conclusions

The presented data reveal that small pH changes within the physiological range can have a large impact on the membrane interactions of porphyrins bearing acidic substituents. Moreover, the strong interdependence of various parameters, namely, pH, aggregation behavior, pK_a values of individual acidic groups, and membrane interactions, was clearly demonstrated. In this respect, NMR spectroscopy provided insight into differences in the qualitative and quantitative aggregation behavior of the pure chlorin compounds as well as into the differently induced membrane perturbations and kinetic behavior, which are all resolved to the submolecular level. Moreover, pK_a values could be assigned to individual acidic groups of the chlorin compounds by ^{13}C NMR.

Even though water-soluble, compounds such as CE, RG, and MACE tend to aggregate in aqueous solution to different extents. The results of this study show that, in general, this feature has to be taken into account when applying water-soluble sensitizers in PDT. Thus, depending on the aggregate size and structure, monomerization of the aggregates (e.g., by delivery systems) may become necessary even for water-soluble drugs to achieve improved membrane incorporation. Nevertheless, moderately stable small aggregates (di/oligomers) may likewise supply sufficient drug material for membrane uptake, maintaining an equilibrium between self-associated and membrane-associated compounds.

Membrane entry and distribution within the membrane were found to be modified in different manners. At lower pH, the entry may be hindered by porphyrin self-association as a competing process whereas increased hydrophobicity significantly enhances membrane translocation. Thus, the strong pH dependence of the membrane distribution was found for those chlorin structures carrying carboxylate groups with pK_a values exclusively in the physiological pH range. The pK_a is therefore an important criterion in the design of membrane-targeting amphiphilic and acidic photosensitizers. Nevertheless, the membrane kinetics of all chlorins reported in this article is in a rather slow regime, suggesting that the cell uptake pathway most likely does not take place via passive diffusion but more likely via endocytosis.

The strong retention in the outer membrane layer found for MACE and also for CE and RG at high pH as a result of electrostatic anchorage in the phospholipid headgroup region may be a preferable property for photosensitizers applied in novel PCI technology. In fact, charged species including chlorin e6 have been reported to exhibit more efficient photoinduced membrane-permeating properties than uncharged ones.[52] For this application, it is also important to note the stability of intravesicular porphyrins, considering the secondary rearrangements that have been proposed in this article to take place at acidic pH over time. Porphyrin self-association reduces phototoxicity and remains a limiting factor that may not be disregarded in any type of application based on PDT.

Acknowledgment. We gratefully acknowledge the financial support obtained from the Swiss National Science Foundation (SNF), grant no. 200021-119691.

(48) Ricchelli, F.; Gobbo, S.; Moreno, G.; Salet, C.; Brancaleon, L.; Mazzini, A. *Eur. J. Biochem.* **1998**, *253*, 760–765.
(49) Borovkov, V. V.; Anikin, M.; Wasa, K.; Sakata, Y. *Photochem. Photobiol.* **1996**, *63*, 477–482.
(50) Pasternack, R. F.; Fleming, C.; Herring, S.; Collings, P. J.; dePaula, J.; DeCastro, G.; Gibbs, E. J. *Biophys. J.* **2000**, *79*, 550–560.
(51) Gorner, H.; Chibisov, A. K.; Slavnova, T. D. *J. Phys. Chem. B* **2006**, *110*, 3917–3923.
(52) Mojzisova, H.; Bonneau, S.; Maillard, P.; Berg, K.; Brault, D. *Photochem. Photobiol. Sci.* **2009**, *8*, 778–787.